2022

Benzothiazole-Substituted Boron Difluoride Formazanate Dyes

Francis L. Buguis

Paul D. Boyle

Joe B. Gilroy
Univeristy of Western Ontario, joe.gilroy@uwo.ca

Benzothiazole-Substituted

Boron Difluoride Formazanate Dyes

Francis L. Buguis, Paul D. Boyle, and Joe B. Gilroy*

Department of Chemistry and The Centre for Advanced Materials and Biomaterials Research (CAMBR), The University of Western Ontario, 1151 Richmond Street North, London, Ontario N6A 5B7 (Canada)

TOC Entry

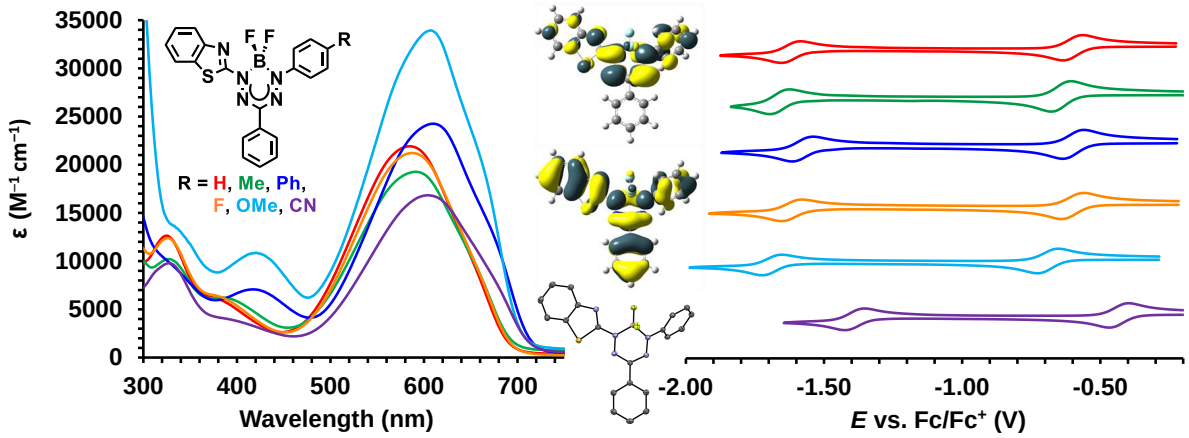

A new family of benzothiazole-containing boron difluoride formazanate dyes are reported. Their substituent-dependent absorption and redox properties reveal that benzothiazole incorporation leads to decreased LUMO levels and narrowed HOMO-LUMO gaps when compared to the benchmark triphenyl-substituted BF_2 formazanate dye.

Keywords

Boron Difluoride Formazanates; Benzothiazole; Heterocycles; Cyclic Voltammetry; Density Functional Theory

Highlights

- A new family of redox-active benzothiazole-substituted BF_2 formazanate dyes were investigated and their properties benchmarked against those of a triphenyl-substituted BF_2 formazanate.

- UV-vis absorption spectroscopy showed that absorption maxima were sensitive to the nature of the *N*-aryl substituents and shifted to lower energies upon benzothiazole incorporation.

- Cyclic voltammetry revealed two reversible reduction events at more positive potentials than those observed for the triphenyl analogue that were altered by variation of the *N*-aryl substituents.

- DFT calculations showed extended conjugation through the benzothiazole and formazanate units and revealed that benzothiazole incorporation led to lowered LUMO levels and narrowed HOMO-LUMO gaps compared to the triphenyl-substituted BF_2 formazanate.

Abstract

The incorporation of benzothiazole heterocycles into existing molecular frameworks has resulted in the production of a wide range of multifunctional molecular materials. However, this strategy has not yet been explored for an emerging class of boron difluoride dyes, derived from formazanate ligands, which often exhibit tuneable redox and optical properties. Here, we address this gap in the literature and describe the synthesis and characterization of a series of benzothiazole-substituted BF_2 formazanates. The incorporation of benzothiazole resulted in absorption profiles that were shifted to lower energies and reduction events that were shifted to more positive potentials when compared to those of the triphenyl-substituted analogue. These results were corroborated by DFT and TD-DFT calculations that suggest that the incorporation of benzothiazole units results in stabilization of the LUMO level thereby narrowing the HOMO-LUMO gaps of this new family of readily accessible dyes. Fine-tuning of these parameters was demonstrated through variation of the supporting *N*-aryl substituents appended to the formazanate ligand backbone.

1. Introduction

Benzothiazole is a heteroaromatic structure that has been used, for example, in chemical biology to introduce bioactivity [1-3] and for biosensing [4, 5], in pharmaceutical chemistry [6], and in the vulcanization of rubber tires [7, 8]. The sulfur (soft Lewis base) and nitrogen (hard Lewis base) atoms have different electron donor characteristics, and the planar five-membered ring serves to extend π-conjugation when coupled to other π-conjugated materials. The incorporation of benzothiazole into molecular frameworks has recently emerged as a useful strategy for the creation of multifunctional materials. The basicity of the benzothiazole nitrogen has proven advantageous for excited-state intramolecular proton transfer (ESIPT), where a phenolic group is typically in close proximity. The shuttling of a proton between ground- and excited-states often leads to turn-on fluorescence, large Stokes shifts, and solvatochromism [9-12]. This basicity also proved useful in colorimetric and fluorescent sensors [13-17], and in dyes that undergo aggregation-induced emission (AIEgens) [18-22].

In the context of this work, the modulation of optoelectronic properties by the addition of benzothiazole substituents is attractive. For example, the substitution of benzothiazole in Rhodol (**I**) [23], as in compound **II**, enables ESIPT and solvatochromism [10]. Boron difluoride complexes of β-ketiminates (**III)** [24], experience enhancement of solid-state emission upon introduction of benzothiazole units, as demonstrated for compound **IV** [25]. Boron difluoride complexes of hydrazone ligands (**V**) are well-studied AIEgens that exhibit large Stokes shifts and bright solid-state emission [26, 27]. By replacing the pyridine moiety with benzothiazole (**VI**), the emission is shifted to lower energies while retaining bright emission [28].

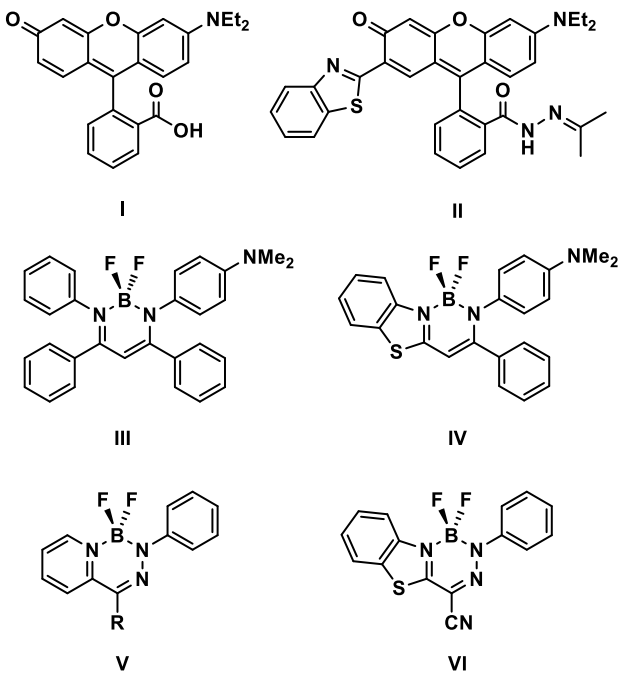

Boron difluoride complexes of readily accessible formazan ligands (BF_2 formazanates, *e.g.* **1**) are an emerging class of dyes that feature tuneable optoelectronic and redox properties [29]. Substituents at the *N*-aryl rings have been shown to significantly affect the absorption, emission, and redox properties of these compounds [30-33]. BF_2 formazanates have demonstrated utility as near-infrared dyes [34, 35], as low band-gap materials [36-38], and as cell imaging agents [39, 40]. Examples of benzothiazole-substituted formazans [41, 42] and their metal complexes [43, 44] have been reported previously, but boron difluoride adducts were unknown prior to this work. Herein, we report the results of an exploratory study of the first examples of BF_2 formazanate dyes bearing benzothiazole substituents.

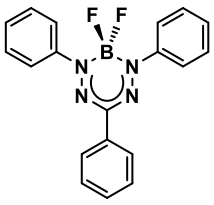

1
BF_2 formazanate

2. Results and Discussion

2.1. Synthesis

The first step in the synthesis of formazans **2a–2f** was the condensation reaction of 2-hydrazinobenzothiazole [17] with benzaldehyde (Scheme 1). The *in situ* generated hydrazone was then combined with the appropriate aryl diazonium chloride salt to afford formazans **2a**–**2f** in yields ranging from 32 to 87% (Fig. S1−12). BF_2 formazanates **3a**–**3f** were synthesized (24−51% yields) by treating the formazans **2a**−**2f** with excess NEt_3 and BF_3•OEt_2 in toluene at reflux. The loss of the diagnostic NH signal (δ: 13.95 to 14.75 for **2a**−**2f**) associated with each formazan in the ^{1}H NMR spectra of the BF_2 adducts indicated the successful transformation to the target compounds. This transformation also led to the appearance of triplets for each compound in the ^{11}B NMR spectra between −0.6 and −0.7 ppm and quartets in the ^{19}F NMR spectra between −137.6 and −138.8 ppm (Fig. S13−S24). The relatively short reaction times (4 h) used to synthesize these benzothiazole-substituted BF_2 formazanates compared to **1** (reaction time = 18 h) [45] was due to the instability of the target compounds at elevated temperatures. In contrast to BF_2 formazanate **1**, which is not prone to hydrolysis, BF_2 formazanates **3a**−**3f** were observed to hydrolyze slowly in solution when exposed to air over periods exceeding 24 h. Despite this sensitivity, we reproducibly synthesized pure samples of formazan **2a**−**2f** and BF_2 formazanates **3a**−**3f** and successfully explored their optoelectronic properties.

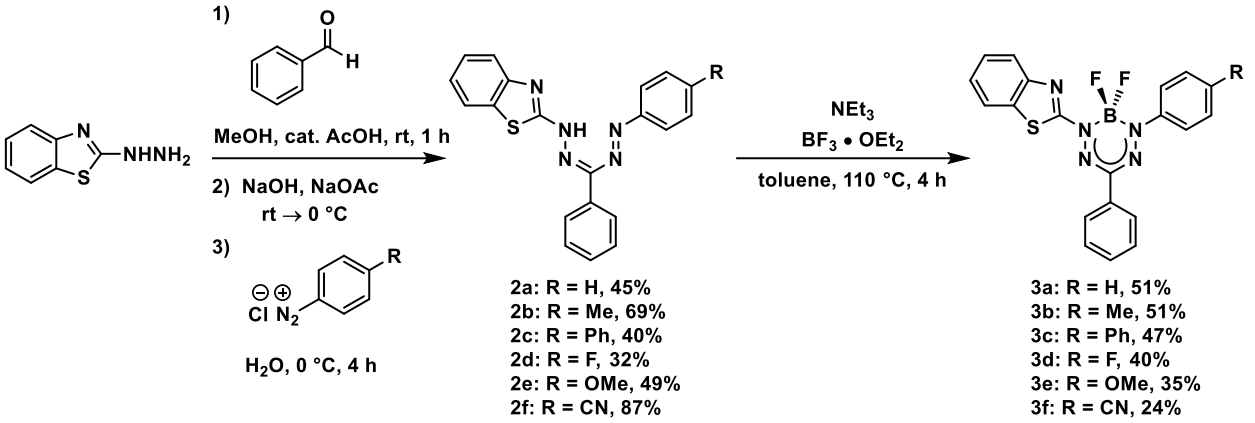

Scheme 1. Synthesis of benzothiazole-substituted formazans and BF_2 formazanate dyes.

2.2. X-ray Crystallography

The solid-state structure of BF_2 formazanate **3a** was determined *via* single-crystal X-ray diffraction (Fig. 1, Tables 1 and S1). It showed that the boron atom, which is displaced from the plane defined by the N_4 atoms of the formazanate backbone by 0.7221(61) Å, adopts a tetrahedral geometry. The N-N [1.2976(16)−1.3271(16) Å] and C-N [1.3295(16)−1.3618(18) Å] bond lengths of the formazanate backbone fell between typical single and double bond lengths of the respective atoms [46]. The N1-C2 bond length [1.4039(18) Å] is slightly shorter than the N3-C9 bond length [1.4328(18) Å]. The benzothiazole substituent was found to be less twisted (α_1 = 20.31º) than the phenyl substituent (α_2 = 55.53º) relative to the plane defined by the N_4 atoms of the formazanate backbone. Taken together, these structural metrics suggest strong electronic delocalization throughout the formazanate ligand backbone and the *N*-aryl substituents.

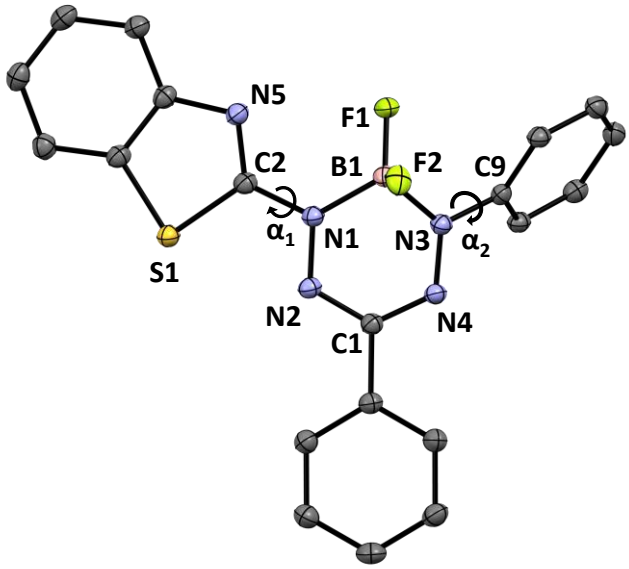

Figure 1. Solid-state structure of BF_2 formazanate dye **3a**. Thermal displacement ellipsoids are shown at 50% probability level. Hydrogen atoms are omitted for clarity.

Table 1. Selected bond lengths, bond angles and structural metrics for BF_2 formazanate dye **3a**. Additional structural refinement data are reported in Table S1.

Metric		**3a**
Bond lengths (Å)	N1−N2	1.3271(16)
	N3−N4	1.2976(16)
	N2−C1	1.3295(17)
	N4−C1	1.3618(18)
	N1−C2	1.4039(18)
	N3−C9	1.4328(18)
	N1−B1	1.557(2)
	N3−B1	1.5780(19)
Bond angles (°)	N2−N1−B1	121.17(11)
	N4−N3−B1	122.14(11)
	N2−C1−N4	124.21(13)
	N1−B1−N3	100.96(10)
Boron displacement (Å)[a]		0.7221(61)
Twist angle α_1 (°)[b]		20.31(5)
Twist angle α_2 (°)[b]		55.53(5)

[a]Distance between the boron and the plane defined by the N_4 backbone. [b]Angles between the planes defined by the *N*-aryl substituents and the N_4 backbone.

2.3. Cyclic Voltammetry

Cyclic voltammetry (CV) experiments conducted in dry CH_2Cl_2 containing [nBu$_4$N][PF_6] as supporting electrolyte revealed two reversible single-electron reduction events for BF_2 formazanates **3a**−**3f** (Fig. 2, Table 2). These reduction events occurred at half-wave potentials of E_{red1}= −0.43 to −0.69 V and E_{red2}= −1.38 to −1.69 V relative to the Fc/Fc^+ redox couple in CH_2Cl_2. In contrast to **1**, which displays reduction events at half-wave potentials of E_{red1}= −0.94 V and E_{red2}= −1.99 V, these benzothiazole-substituted compounds are reduced at more positive potentials, indicating lower LUMO energies. Similar to other BF_2 formazanates, reduction takes place at the BF_2 formazanate backbone and corresponds to the conversion of the neutral dyes to their respective radical anion and dianion (Scheme 2) [33]. Compared to compound **3a** (R = H), the introduction of an electron-donating group, such as in compounds **3b** (R = Me), **3c** (R = Ph), and **3e** (R = OMe), shifted the reduction events to more positive potentials. Incorporating an electron-withdrawing group, such as in compound **3f** (R = CN), shifted these events to more negative potentials, while a weaker withdrawing group, such as in compound **3d (**R = F), did not drastically affect these reduction potentials. We did not observe any oxidation features within the electrochemical stability window of CH_2Cl_2.

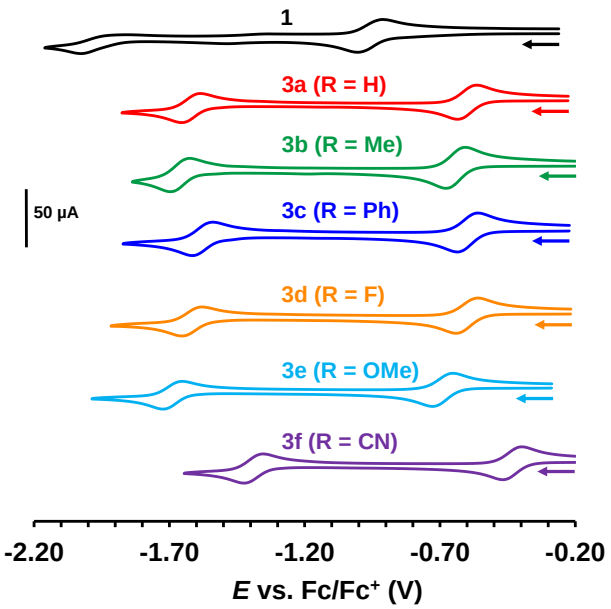

Figure 2. Cyclic voltammograms recorded for dry, degassed 1 mM solutions of BF_2 formazanate dyes **1** and **3a**–**3f** in CH_2Cl_2 containing 0.1 M [*n*Bu_4N][PF_6] as supporting electrolyte at a scan rate of 250 mV s^{-1}. The arrows indicate the initial scan direction.

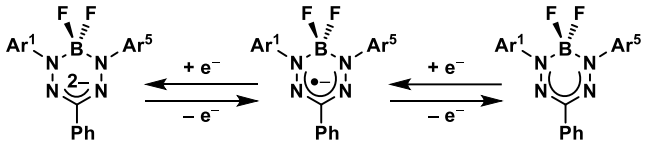

Scheme 2. Stepwise reduction of BF_2 formazanate dyes to their respective radical anion and dianion forms.

2.4. UV-vis Absorption Spectroscopy

UV-vis absorption spectroscopy experiments revealed that the absorption bands of BF_2 formazanates **3a**–**3f** appeared at lower energies relative to those of compound **1** (Fig. 3 and S25, Table 2). For example, the addition of a benzothiazole substituent, such as in **3a** (λ_{max} = 585 nm in toluene) shifted the absorption band to lower energy compared to **1** (λ_{max} = 517 nm in toluene). Compounds **3b** (R = Me, λ = 593 nm in toluene), **3c** (R = Ph, λ_{max} = 611 nm in toluene), and **3e** (R = OMe, λ_{max} = 607 nm in toluene) experienced the largest changes in low-energy absorption maxima due to the electron-donating ability of the *p*-substituent and the extension of π-

conjugation. Consistent with the cyclic voltammetry experiments, the introduction of a fluorine-substituent in compound **3d** (λ_{max} = 588 nm in toluene) resulted in minimal change (Fig. 3) when compared to compound **3a**. The absorption profiles of BF_2 formazanates **3a**–**3f** are insensitive to solvent polarity ($\Delta\lambda_{max}$ = 10–15 nm in toluene, CH_2Cl_2, and THF) indicating the low energy transitions do no involve charge transfer. These compounds are non-emissive in solution and in the solid-state, which is typical of BF_2 formazanates with *C*-aryl substituents [45].

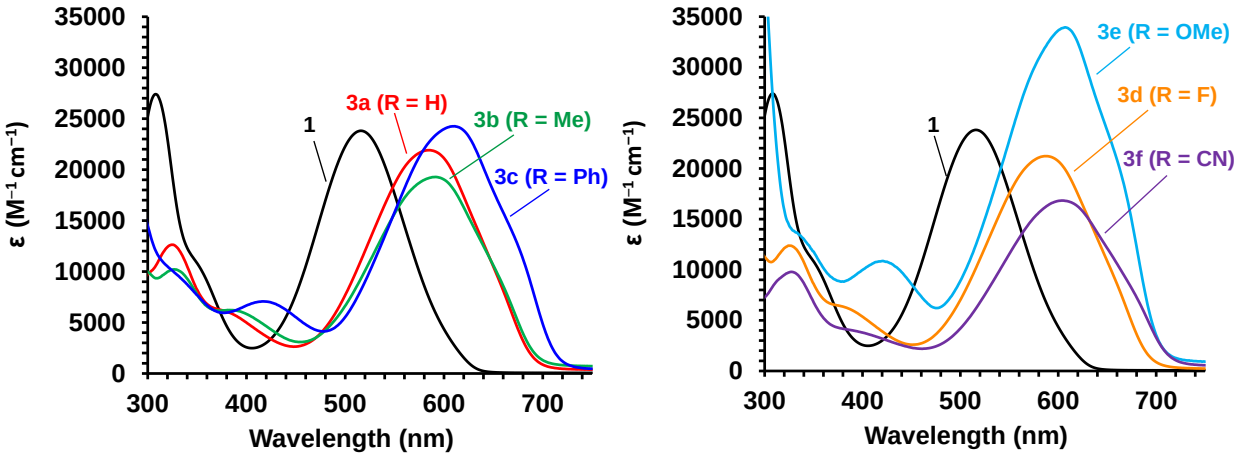

Figure 3. UV-vis absorption spectra of BF_2 formazanate dyes **1** and **3a**–**3f** recorded for 10^{-6} M solutions in toluene.

Table 2. Experimental and calculated solution-state characterization data for BF_2 formazanate dyes **1** and **3a**–**3f**. The theoretical values were obtained using TDDFT at the M06/6-311+G* SCRF=PCM level.

	Experimental				Theoretical
	λ_{max} (nm)	ε (M^{-1} cm^{-1})	E_{red1} (V)[a]	E_{red2} (V)[a]	λ_{abs} (nm)
1[45]					
toluene	517	23800			496
CH_2Cl_2	509	23400	–0.94	–1.99	
THF	509	22500			
3a (R = H)					
toluene	585	21000			568
CH_2Cl_2	580	22500	–0.60	–1.62	
THF	572	21600			
3b (R = Me)					
toluene	593	18200			585
CH_2Cl_2	588	18600	–0.64	–1.66	
THF	579	15300			
3c (R = Ph)					
toluene	611	24300			609
CH_2Cl_2	607	28000	–0.60	–1.58	
THF	596	25500			
3d (R = F)					
toluene	588	20800			572
CH_2Cl_2	583	24000	–0.59	–1.62	
THF	575	21800			
3e (R = OMe)					
toluene	607	32200			609
CH_2Cl_2	605	25700	–0.69	–1.69	
THF	596	28000			
3f (R = CN)					
toluene	605	16100			606
CH_2Cl_2	599	23000	–0.43	–1.38	
THF	590	21400			

[a]CV experiments were performed in dry, degassed 1 mM CH_2Cl_2 solutions containing 0.1 M [*n*Bu_4N][PF_6] as supporting electrolyte at a scan rate of 250 mV s^{-1}. Data were referenced internally to the ferrocene/ferrocenium redox couple.

2.5. DFT and TDDFT Studies

To better understand the optoelectronic properties of BF_2 formazanates **3a**−**3f**, time-dependent density-functional theory (TDDFT) calculations were performed at the M06/6-311+G* level of theory with equilibrium solvation. The HOMOs and LUMOs for compounds **3a**, **3e** and **3f** are depicted in Figure 4, while similar data can be found for **1**, **3b**, **3c** and **3d** in Figure S26. The TDDFT calculations implicate the highest occupied molecular orbital (HOMO, π-type) and lowest unoccupied molecular orbital (LUMO, π*-type) in the lowest-energy transitions for each compound and the theoretical low-energy absorptions are in good agreement with experimental values (Table 2). The optimized ground-state geometries show that both the HOMO and LUMO are delocalized through the BF_2 formazanate backbone (Fig. 4 and S26). The benzothiazole substituent also shows electronic contribution, suggesting that the presence of this heterocycle has a significant effect on the optoelectronic properties of these BF_2 formazanates.

The HOMO-LUMO gaps (E_g) of BF_2 formazanates **1** and **3a**–**3f** were obtained from the optimized structures (Fig. 5). Comparing compounds **1** (E_g = 3.15 eV) and **3a** (E_g = 2.80 eV), it is evident that incorporating a benzothiazole ring significantly stabilized the LUMO level. The resulting narrowed HOMO-LUMO gap corroborates the CV and UV-vis absorption experiments. Next, comparing the benzothiazole-substituted compounds, the substitution of strongly donating (**3e**, R = OMe) and withdrawing (**3f**, R = CN) groups imparted the largest change in the HOMO-LUMO gaps at 2.63 eV and 2.65 eV, respectively. Extending the conjugation, as in **3c** (R = Ph), had a similar effect (E_g = 2.65 eV) in narrowing the HOMO-LUMO gap, while weakly donating (**3b**, R = Me), and withdrawing (**3d**, R = F) groups had mild effects with E_gs of 2.73 eV and 2.78 eV, respectively.

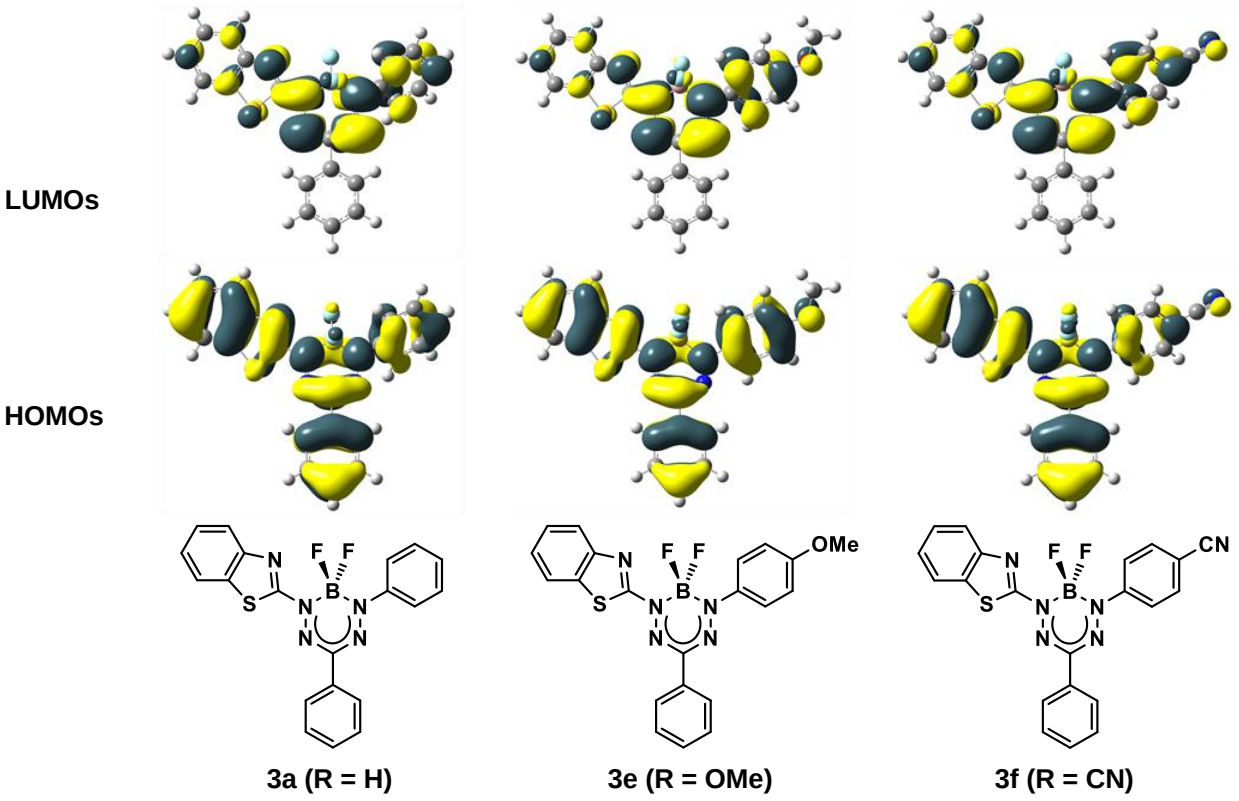

Figure 4. Frontier molecular orbitals of BF_2 formazanate dyes **3a**, **3e**, and **3f** calculated at the ground-state geometries using M06/6-311+G* SCRF = (PCM, solvent = toluene) method.

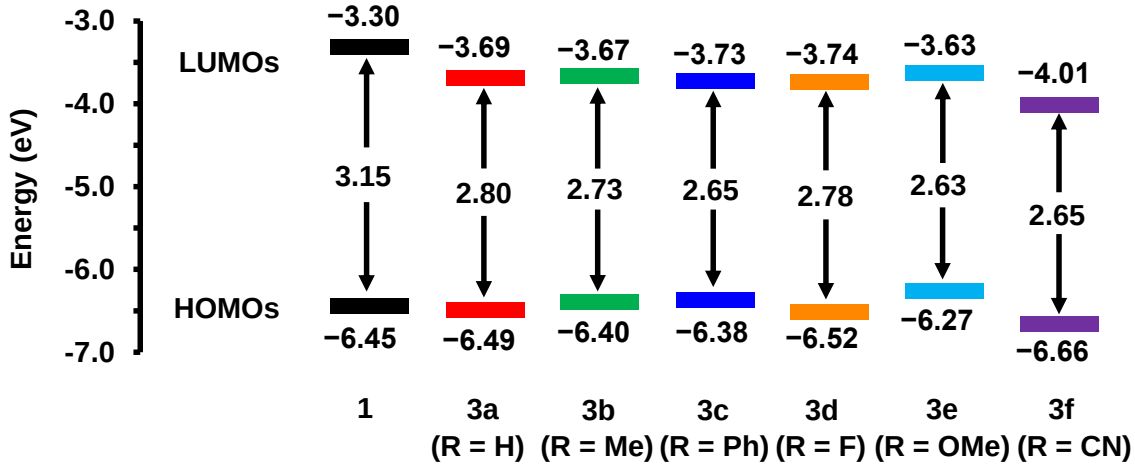

Figure 5. HOMO and LUMO energies of BF_2 formazanate dyes **1** and **3a**−**3f** calculated at M06/6-311+G* SCRF = (PCM, solvent = toluene) level of theory.

3. Conclusions

A series of benzothiazole-substituted formazans (**2a**−**2f**) and their corresponding BF_2 adducts (**3a**−**3f**) were synthesized, and their optoelectronic properties examined. The absorption maxima of BF_2 formazanates **3a**−**3f** shifted to lower energies compared to the phenyl-substituted analogue **1**. These results suggest that dyes **3a**−**3f** possess narrower HOMO-LUMO gaps, likely due to stabilized LUMOs, as shown by cyclic voltammetry experiments. Our TDDFT calculations corroborate the experimental observations and confirm LUMO stabilization, highlighting the effects of benzothiazole incorporation on the properties of BF_2 formazanates, thus expanding the design criteria for far-red dyes. Finally, reduction potentials and HOMO-LUMO gaps can be rationally fine-tuned by varying the *N*-aryl substituents. Substituent variation at the benzothiazole ring and the carbon of the formazanate ring are the next logical steps in optimizing the properties of a new family of multifunctional heterocycles and will be described in due course.

Declaration of Conflict of Interest

The authors declare no known conflict of interest that could have influenced the work reported in this paper.

Author Contributions

F.L.B. and J.B.G. designed the experiment. F.L.B. synthesized and characterized the data reported and wrote a draft of the manuscript. P.D.B. collected and refined X-ray diffraction data. J.B.G. edited the manuscript and handled its submission.

Acknowledgements

This work was supported by the Natural Sciences and Engineering Research Council (NSERC) of Canada (F.L.B: CGS-D Scholarship; J.B.G.: DG, RGPIN-2018-04240), the Ontario Ministry of Research and Innovation (J.B.G.: ERA, ER-14-10-147), and the Canadian Foundation for Innovation (J.B.G.: JELF, 33977). We would like to thank the facilities of Compute/Calcul Canada (www.computecanada.ca) for allowing us to run theoretical calculations.

References

[1] Mokesch S, Cseh K, Geisler H, Hejl M, Klose MHM, Roller A, et al. Investigations on the anticancer potential of benzothiazole-based metallacycles. Front Chem. 2020;8:209.

[2] Chander Sharma P, Sharma D, Sharma A, Bansal KK, Rajak H, Sharma S, et al. New horizons in benzothiazole scaffold for cancer therapy: Advances in bioactivity, functionality, and chemistry. Appl Mater Today. 2020;20:100783.

[3] Sultana F, Saifi MA, Syed R, Mani GS, Shaik SP, Osas EG, et al. Synthesis of 2-anilinopyridyl linked benzothiazole hydrazones as apoptosis inducing cytotoxic agents. New J Chem. 2019;43(18):7150–61.

[4] Zhou X, Mandal S, Jiang S, Lin S, Yang J, Liu Y, et al. Efficient long-range, directional energy transfer through DNA-templated dye aggregates. J Am Chem Soc. 2019;141(21):8473–81.

[5] Liu Q, Zhang C, Wang X, Gong S, He W, Liu Z. Benzothiazole-pyimidine-based BF_2 complex for selective detection of cysteine. Chem Asian J. 2016;11(2):202–6.

[6] Keri RS, Patil MR, Patil SA, Budagumpi S. A comprehensive review in current developments of benzothiazole-based molecules in medicinal chemistry. Eur J Med Chem. 2015;89:207–51.

[7] Zhang J, Zhang X, Wu L, Wang T, Zhao J, Zhang Y, et al. Occurrence of benzothiazole and its derivates in tire wear, road dust, and roadside soil. Chemosphere. 2018;201:310–7.

[8] Engels H-W, Weidenhaupt H-J, Pieroth M, Hofmann W, Menting K-H, Mergenhagen T, et al. Rubber, 9. Chemicals and Additives. Ullmann's Encyclopedia of Industrial Chemistry2011.

[9] Ren H, Huo F, Wu X, Liu X, Yin C. An ESIPT-induced NIR fluorescent probe to visualize mitochondrial sulfur dioxide during oxidative stress in vivo. Chem Commun. 2021;57(5):655–8.

[10] Liu X, Li A, Xu W, Ma Z, Jia X. An ESIPT-based fluorescent switch with AIEE, solvatochromism, mechanochromism and photochromism. Mater Chem Front. 2019;3(4):620–5.

[11] Sedgwick AC, Wu L, Han HH, Bull SD, He XP, James TD, et al. Excited-state intramolecular proton-transfer (ESIPT) based fluorescence sensors and imaging agents. Chem Soc Rev. 2018;47(23):8842–80.

[12] Tsuchiya S, Sakai KI, Kawano K, Nakane Y, Kikuchi T, Akutagawa T. Color changes of a full-color emissive ESIPT fluorophore in response to recognition of certain acids and their conjugate base anions. Chem Eur J. 2018;24(22):5868–75.

[13] Huang Z, Zhou C, Chen W, Li J, Li M, Liu X, et al. A polymerizable aggregation induced emission (AIE)-active dye with remarkable pH fluorescence switching based on benzothiazole and its application in biological imaging. Dyes Pigm. 2021;196:109793.

[14] Sadek O, Galan LA, Gendron F, Baguenard B, Guy S, Bensalah-Ledoux A, et al. Chiral benzothiazole monofluoroborate featuring chiroptical and oxygen-sensitizing properties: synthesis and photophysical studies. J Org Chem. 2021;86(17):11482–91.

[15] Coelho FL, da Costa Duarte R, de Ávila Braga C, Toldo JM, Bruno Gonçalves PF, da Silveira Santos F, et al. Benzothiazole merocyanine dyes as middle pH optical sensors. Dyes Pigm. 2020;176:108193.

[16] Jin Y, Wang S, Zhang Y, Song B. Highly selective fluorescent chemosensor based on benzothiazole for detection of Zn^{2+}. Sens Actuators B Chem. 2016;225:167–73.

[17] Tang H-Y, Gao Y, Li B, Li C-W, Guo Y. Reaction-based colorimetric and ratiometric fluorescent probe for highly selective detection of silver ions. Sens Actuators B Chem. 2018;270:562–9.

[18] Gong S-S, Kong R, Zheng C, Fan C, Wang C, Yang D-Z, et al. Multicomponent reaction-based discovery of pyrimido[2,1-b][1,3]benzothiazole (PBT) as a novel core for full-color-tunable AIEgens. J Mater Chem C. 2021;9(31):10029–36.

[19] Potopnyk MA, Volyniuk D, Luboradzki R, Lazauskas A, Grazulevicius JV. Aggregation-induced emission-active carbazolyl-modified benzo[4,5]thiazolo[3,2-c]oxadiazaborinines as mechanochromic fluorescent materials. Eur J Org Chem. 2021;2021(19):2772–81.

[20] Singh VD, Dwivedi BK, Kumar Y, Pandey DS. Artificial light-harvesting systems (LHSs) based on boron-difluoride (BF2) hydrazone complexes (BODIHYs). New J Chem. 2021;45(3):1677–85.

[21] Niu Y, Wang R, Shao P, Wang Y, Zhang Y. Nitrostyrene-modified 2-(2-hydroxyphenyl)benzothiazole: enol-emission solvatochromism by ESICT-ESIPT and aggregation-induced emission enhancement. Chem Eur J. 2018;24(62):16670–6.

[22] Li K, Feng Q, Niu G, Zhang W, Li Y, Kang M, et al. Benzothiazole-based AIEgen with tunable excited-state intramolecular proton transfer and restricted intramolecular rotation processes for highly sensitive physiological pH sensing. ACS Sens. 2018;3(5):920–8.

[23] Poronik YM, Vygranenko KV, Gryko D, Gryko DT. Rhodols - synthesis, photophysical properties and applications as fluorescent probes. Chem Soc Rev. 2019;48(20):5242–65.

[24] Yoshii R, Hirose A, Tanaka K, Chujo Y. Functionalization of boron diiminates with unique optical properties: multicolor tuning of crystallization-induced emission and introduction into the main chain of conjugated polymers. J Am Chem Soc. 2014;136(52):18131–9.

[25] Liu Q, Wang X, Yan H, Wu Y, Li Z, Gong S, et al. Benzothiazole-enamide-based BF2 complexes: luminophores exhibiting aggregation-induced emission, tunable emission and highly efficient solid-state emission. J Mater Chem C. 2015;3(12):2953–9.

[26] Cappello D, Therien DAB, Staroverov VN, Lagugné-Labarthet F, Gilroy JB. Optoelectronic, aggregation, and redox properties of double-rotor boron difluoride hydrazone dyes. Chem Eur J. 2019;25(23):5994–6006.

[27] Yang Y, Su X, Carroll CN, Aprahamian I. Aggregation-induced emission in BF2–hydrazone (BODIHY) complexes. Chem Sci. 2012;3(2):610–3.

[28] Duan W, Liu Q, Huo Y, Cui J, Gong S, Liu Z. AIE-active boron complexes based on benzothiazole-hydrazone chelates. Org Biomol Chem. 2018;16(27):4977–84.

[29] Gilroy JB, Otten E. Formazanate coordination compounds: synthesis, reactivity, and applications. Chem Soc Rev. 2020;49(1):85–113.

[30] Chang M-C, Chantzis A, Jacquemin D, Otten E. Boron difluorides with formazanate ligands: redox-switchable fluorescent dyes with large stokes shifts. Dalton Trans. 2016;45(23):9477–84.

[31] Barbon SM, Reinkeluers PA, Price JT, Staroverov VN, Gilroy JB. Structurally Tunable 3-Cyanoformazanate Boron Difluoride Dyes. Chem Eur J. 2014;20(36):11340–4.

[32] Barbon SM, Price JT, Reinkeluers PA, Gilroy JB. Substituent-Dependent Optical and Electrochemical Properties of Triarylformazanate Boron Difluoride Complexes. Inorg Chem. 2014;53(19):10585–93.

[33] Chang M-C, Otten E. Synthesis and ligand-based reduction chemistry of boron difluoride complexes with redox-active formazanate ligands. Chem Commun. 2014;50(56):7431–3.

[34] Buguis FL, Maar RR, Staroverov VN, Gilroy JB. Near-infrared boron difluoride formazanate dyes. Chem Eur J. 2021;27(8):2854–60.

[35] Maar RR, Zhang R, Stephens DG, Ding Z, Gilroy JB. Near-Infrared Photoluminescence and Electrochemiluminescence from a Remarkably Simple Boron Difluoride Formazanate Dye. Angew Chem Int Ed. 2019;58(4):1052–6.

[36] Dhindsa JS, Buguis FL, Anghel M, Gilroy JB. Band gap engineering in acceptor-donor-acceptor boron fifluoride formazanates. J Org Chem. 2021;86(17):12064–74.

[37] Kawano Y, Ito Y, Ito S, Tanaka K, Chujo Y. π-Conjugated copolymers composed of boron formazanate and their application for a wavelength converter to bear-infrared light. Macromolecules. 2021;54(4):1934–42.

[38] Dhindsa JS, Maar RR, Barbon SM, Olivia Avilés M, Powell ZK, Lagugné-Labarthet F, et al. A π-conjugated inorganic polymer constructed from boron difluoride formazanates and platinum(ii) diynes. Chem Commun. 2018;54(50):6899–902.

[39] Sharma N, Barbon SM, Lalonde T, Maar RR, Milne M, Gilroy JB, et al. The development of peptide–boron difluoride formazanate conjugates as fluorescence imaging agents. RSC Adv. 2020;10(32):18970–7.

[40] Maar RR, Barbon SM, Sharma N, Groom H, Luyt LG, Gilroy JB. Evaluation of Anisole-Substituted Boron Difluoride Formazanate Complexes for Fluorescence Cell Imaging. Chem Eur J. 2015;21(44):15589–99.

[41] Fedorchenko TG, Lipunova GN, Shchepochkin AV, Tsmokalyuk AN, Valova MS, Slepukhin PA. Synthesis, spectral and electrochemical properties of halogenated 6-alkyl-5-aryl-1-(benzo[d]thiazol-2-yl)-3-phenylverdazyls and 5-aryl-1-(benzo[d]thiazol-2-yl)-3-phenyl-6-vinylverdazyls. Chem Heterocycl Compd. 2019;55(6):560–5.

[42] Bednyagina NP, Lipunova GN. The structure of unsymmetrical formazans of the benzazole series. Chem Heterocycl Compd. 1969;5:877–81.

[43] Zaidman AV, Khasbiullin II, Belov GP, Pervova IG, Lipunov IN. Catalytic activity of new nickel(II) formazanates in ethylene oligomerization. Pet Chem. 2012;52(1):28–34.

[44] Kessenikh AV, Shmelev LV. Chemical shifts and spin-spin couplings of the metal nuclei with the carbon 13C nuclei in the ligand in mercury and cadmium bisheteroarylformazanates. Chem Heterocycl Compd. 1995;31(9):1122–31.

[45] Barbon SM, Staroverov VN, Gilroy JB. Effect of Extended π Conjugation on the Spectroscopic and Electrochemical Properties of Boron Difluoride Formazanate Complexes. J Org Chem. 2015;80(10):5226–35.

[46] Haynes WM, Lide DR, Bruno TJ. CRC Handbook of Chemistry and Physics. 97 ed. Boca Raton, Florida: CRC Press, 2016.